Progress In Electromagnetics Research C, Vol. 55, 105–113, 2014

Broadband Dual Polarized Space-Fed Antenna Arrays with High Isolation

Prashant K. Mishra[1, *], Dhananjay R. Jahagirdar[1], and Girish Kumar[2]

Abstract—This paper presents a novel design of dual polarized space-fed antenna arrays with broad bandwidth and high isolation between two orthogonal ports. The dual polarized space-fed antenna arrays are designed with bottom radiating element electromagnetically coupled to two orthogonal open microstrip lines and top parasitic elements excited by the radiation from bottom radiating element, without any feed network for array elements excitation. Two space-fed antenna arrays with 7 and 19 parasitic elements, respectively, have been designed for 5.8 GHz frequency band and their performances are analyzed. The dual polarized space-fed array with 19 parasitic elements has been fabricated, and its performance is measured. The measured impedance bandwidth is 10.7%, isolation ≥ 32 dB between two orthogonal ports over entire bandwidth, maximum gain of 17.8 dBi and cross-polar levels ≤ -29 dB.

1. INTRODUCTION

With increasing demand of bandwidth intensive services for wireless communication and network systems, there is emphasis on improving link reliability and channel capacity of these systems. To achieve this, various diversity techniques have been proposed. Two diversity techniques, i.e., space and polarization diversity, are employed using antennas. In space diversity, multiple antennas are used for transmission and reception. The polarization diversity is achieved using two orthogonal ports of the same antenna. With miniaturization of communication systems and devices, the polarization diversity has become attractive as it requires less space than space diversity.

The dual polarized antennas are used in cellular base stations, multiple input multiple output (MIMO) systems for WiMAX applications and in radar systems [1–5]. Use of polarization diversity in MIMO system provides improved multiplexing gains, especially in Rayleigh fading channels and in the presence of high transmit fading signal correlation [2]. Dual polarized antennas for MIMO systems also provide improved channel capacity as compared to single polarized antennas [3]. The dual polarized antennas are used in radars to get information in horizontal and vertical planes simultaneously [4, 5].

To cater for these requirements, it is important to achieve broad bandwidth and high isolation between two orthogonal ports in dual polarized antennas. Various feed techniques of dual polarized antennas such as capacitive probe feed, aperture coupled, gap feed and hybrid feed have been proposed to achieve broad bandwidth and to improve isolation between two orthogonal ports [6–13]. A dual polarized antenna with two L-shaped probes achieves maximum isolation of 20 dB [6]. Antenna with dual meandering probes has impedance bandwidth of 26% with isolation ≥ 25 dB [7]. To improve isolation of aperture coupled antennas, various configurations with different slot shapes have been proposed. In [8], dog bone shaped slots are used, which results in better coupling to radiating element and reduction in slot dimension achieving isolation ≥ 30 dB. Dual polarized antenna with 'H' shaped

Received 27 October 2014, Accepted 1 December 2014, Scheduled 10 December 2014

* Corresponding author: Prashant Kumar Mishra (mishra.pk81@gmail.com).

[1] Research Center Imarat, Defence Research & Development Organisation, Hyderabad 500069, India. [2] Department of Electrical Engineering, Indian Institute of Technology Bombay, Mumbai 400076, India.

coupling slots arranged in 'T' configuration [9] and with modified 'H' shaped slots [10] have been proposed achieving isolation ≥ 30 dB. However, aperture coupled antennas have high back lobe radiation due to microstrip feed network placed at the bottom of the ground plane. The back lobe radiation can be suppressed by placing an additional layer with reflector at the bottom of feed network, but the isolation between two ports is reduced due to reflection from reflector. The dual polarized antennas have also been designed using coaxial feed for one port and aperture coupled feed for second port. These antenna configurations have isolation ≥ 30 dB, but the cross-polar levels are ≤ -20 dB. In [13], dual polarized antenna is designed using gap-fed microstrip radiating element achieving isolation ≥ 30 dB and impedance bandwidth of 5% at 14.9 GHz.

To achieve higher gain and narrow beam coverage, various designs of dual polarized antenna arrays have been proposed [14–21]. Array of 16 corner-fed microstrip elements with feed network has been proposed in [14], achieving impedance bandwidth of 4%, isolation ≥ 30 dB and cross-polar levels ≤ -22 dB. A broadband dual polarized microstrip antenna array with slot coupled feed and microstrip line feed for two polarizations is proposed in [15]. The 4 element array achieves bandwidth of 14% with isolation ≥ 30 dB and cross-polar levels ≤ -20 dB. In [16], the 2×1 L-probe stacked patch array is designed with dual feed network to suppress the coupling. The antenna array achieves bandwidth of 19.8% for return loss ≤ 14 dB and isolation ≥ 36 dB, however the cross-polar levels are poor due to radiation from feed network. The 16 element planar array with radiating elements and matching network designed on two substrate layers has been proposed in [17], achieving isolation ≥ 40 dB. In [18], 36 element dual polarized planar antenna array is proposed using electromagnetically coupled elements and feed network, achieving impedance bandwidth $\geq 26\%$ and isolation ≥ 30 dB. The 4×2 dual polarized shared aperture antenna array is designed in [19], using linear and bent slots achieving ≥ 30 dB isolation and cross-polar levels ≤ -25 dB. In [20], 2×2 dual polarized antenna array for LTE frequency band has been designed using planar structures on single substrate with isolation ≥ 30 dB and cross-polar levels ≤ -22 dB. The 16×1 dual polarized array for Wi-Fi/WiMAX, with bottom rectangular elements and top parasitic cones has been proposed in [21]. The antenna array has 20% bandwidth with isolation ≥ 20 dB and cross-polar levels ≤ -19.2 dB.

In this paper, design of broadband dual polarized antenna array is proposed using top layer parasitic elements excited by radiation from bottom radiating element to achieve high gain. The bottom radiating element is electromagnetically coupled to two orthogonal microstrip feed lines for dual polarization. The proposed antenna design results in improved isolation as no feed network is used for the design of high gain arrays.

2. DUAL POLARIZED SPACE-FED ANTENNA ARRAY DESIGN

The dual polarized space-fed antenna arrays are designed using circular microstrip antenna (CMSA) for 5.8 GHz frequency band. The dual polarized space-fed antenna array consists of two substrate layers. Bottom substrate layer of $\epsilon_r = 2.55$, $h = 0.787$ mm and $\tan\delta = 0.0015$ is used for feed design of two orthogonal ports. To reduce cost, glass epoxy substrate of $\epsilon_r = 4.4$, $h = 0.8$ mm and $\tan\delta = 0.02$ is used for top substrate layer consisting of array of parasitic elements. Two configurations of dual polarized space-fed antenna array are designed with 1 radiating and 7 parasitic elements (1B7T) and 1 radiating and 19 parasitic elements (1B19T).

The configuration of 1B19T dual polarized space-fed antenna array is shown in Figure 1. Bottom substrate layer consists of two orthogonal open microstrip feed lines of length l_1 and width w_1 placed with a spacing of s from center as shown in Figure 2. To achieve $50\,\Omega$ impedance matching, each microstrip line is connected to a quarter wave transformer of length l_2 and width w_2. The bottom CMSA radiating element of radius r is placed at a height h_1 from microstrip feed lines in suspended configuration. The CMSA is electromagnetically coupled to two orthogonal microstrip feed lines achieving dual linear polarization. Array of CMSA parasitic elements are designed on a superstrate at a height h_2 from bottom radiating element and are placed in inverted microstrip configuration. For space-fed antenna arrays, as number of elements increases, the parasitic element height is increased to ensure that all the parasitic elements are having sufficient excitation. The array of parasitic elements has one CMSA of radius r_1 at the center and other elements are arranged in a concentric circle around the central element. For 1B7T configuration, 6 CMSA of radius r_2 are arranged in concentric circle at a spacing of s_1 from

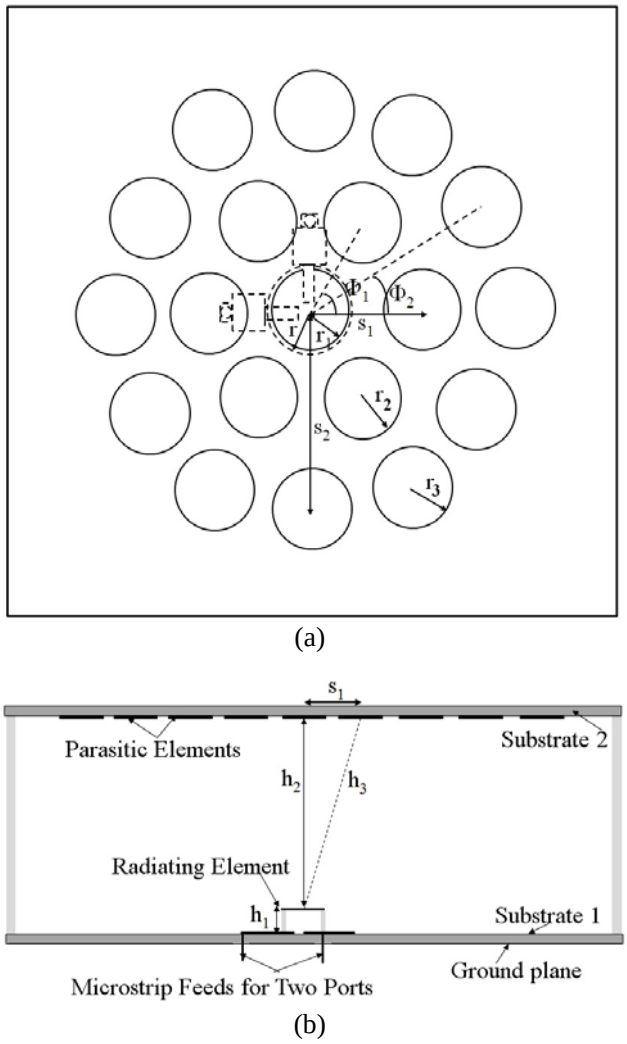

Figure 1. 1B19T dual polarized space-fed antenna array, (a) top and (b) side views (not to the scale).

central element and an equal inter-element angular spacing of $\phi_1 = 60$ degrees among elements. The 1B19T antenna array is designed by placing additional 12 elements of radius r_3 in second concentric circle at a spacing of s_2 from central element and with angular separation of $\phi_2 = 30$ degrees among elements. The dimensions of 1B7T and 1B19T dual polarized space-fed antenna arrays are summarized in Table 1.

For space-fed antenna array, the parasitic elements are excited by the radiation from bottom radiating element. The distances of parasitic elements arranged at different concentric circles from bottom radiating patch are different, so these are excited with a phase difference. If central parasitic element is placed at a distance h_2 and outer elements in first concentric circle are placed at distance h_3 from bottom radiating element, then the phase difference e_θ between them is given by

$$e_\theta = \frac{2\pi * a}{\lambda_0} \tag{1}$$

where λ_0 is free space wavelength and a is the difference in distance between two parasitic elements from bottom radiating element, which is calculated as

$$a = h_3 - h_2 \tag{2}$$

$$\text{where } h_3 = \sqrt{\left(h_2^2 + s_1^2\right)} \tag{3}$$

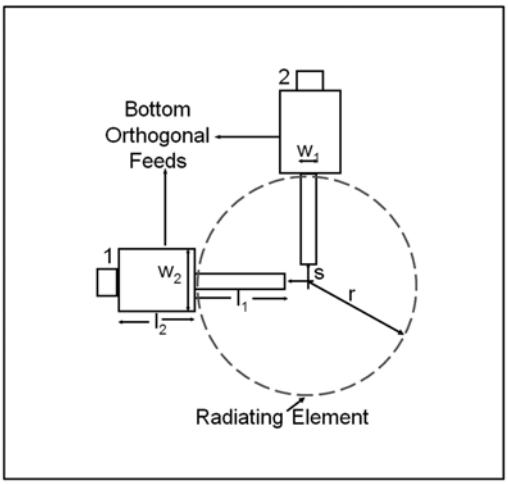

Figure 2. Dual microstrip feed line configuration with quarter wave transformer of dual polarized space-fed antenna array.

Table 1. Dimensions of 1B7T and 1B19T dual polarized space-fed antenna arrays.

Parameters	1B7T Array (mm)	1B19T Array (mm)
Microstrip feed line dimensions ($l_1 \times w_1$)	7.7×1	7.45×1
Quarter wave transformer dimensions ($l_2 \times w_2$)	8.8×12.2	8.8×10.2
Microstrip feed lines offset (s)	2.8	2.4
Bottom radiating element radius (r)	10.8	10.8
Radiating element spacing from ground plane (h_1)	3	2.5
Central parasitic element radius (r_1)	10.7	10.6
First concentric circle elements radius (r_2)	10.4	10.3
Second concentric circle elements radius (r_3)	-	10
Parasitic arrays inter element spacing (s_1, s_2)	33, -	33, 66
Parasitic elements spacing from bottom radiating element (h_2)	25.85 ($\lambda_0/2$)	77.55 ($3\lambda_0/2$)
Ground plane dimension	130×130	200×200

Similarly, the phase difference for the elements in subsequent concentric circles can be calculated. The parasitic elements arranged in concentric circles have advantage that all the elements have same distance from bottom radiating element. This results in same phase difference among all the elements, resulting in simpler phase compensation requirement. In the proposed design, the radius of parasitic elements in outer concentric circles are gradually reduced to achieve phase compensation among all the parasitic elements. The variation of reflection coefficient phase with respect to change in radius of circular element is analyzed as shown in Figure 3 and is used for determining the radius of outer parasitic elements. The parasitic elements with reduced radius have capacitive reflection coefficient phase, which compensates the phase difference in outer parasitic elements. The reflection coefficient phase slope is nonlinear with higher variation at the resonance and low variation for nonresonant radius of circular elements. For phase compensation, the phase difference is calculated and radius of parasitic circular elements in each concentric circle is determined from reflection coefficient phase variation. Since reflection coefficient phase has different variation for different frequencies, the phase compensation is done for center frequency.

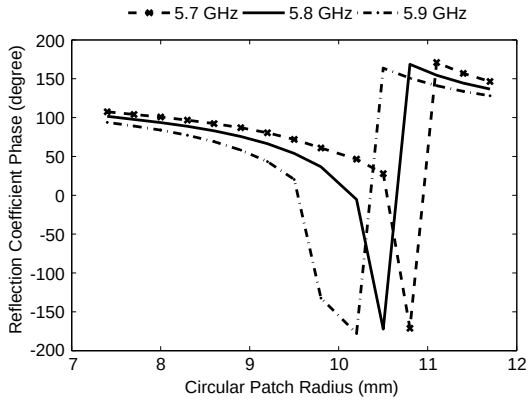

Figure 3. Reflection coefficient phase variation with respect to change in circular patch radius.

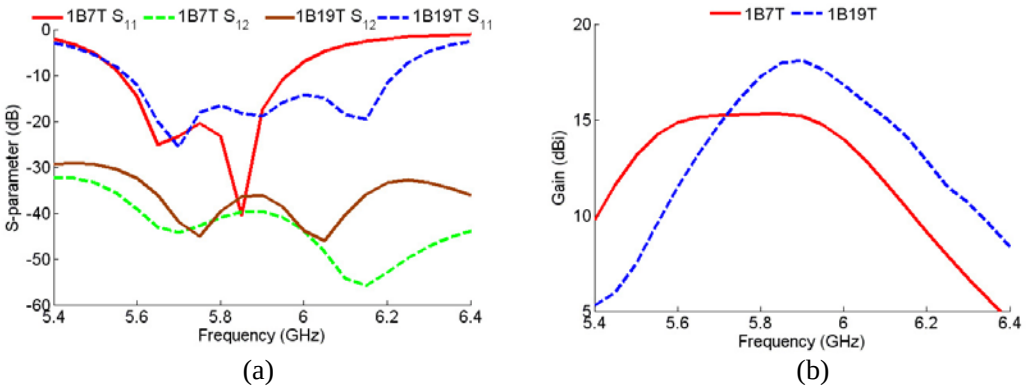

(a) (b)

Figure 4. Simulated (a) S-parameters and (b) gain vs. frequency plots for port1 of 1B7T and 1B19T dual polarized space-fed antenna arrays.

3. SIMULATED AND MEASURED RESULTS

The 1B7T and 1B19T dual polarized space-fed antenna array configurations are analyzed using IE3D [22]. Simulated S-parameters vs. frequency plots for port1 of 1B7T and 1B19T dual polarized space-fed arrays are shown in Figure 4(a). The 1B7T antenna array has return loss (RL) ≤ 10 dB from 5.56 to 5.96 GHz, achieving 7% bandwidth. The 1B19T antenna array has RL ≤ 10 dB from 5.58 to 6.22 GHz, achieving 11% bandwidth. The reduction in radius of outer circular parasitic elements in space-fed antenna results in array of staggered resonators, achieving broad bandwidth. The isolation between two orthogonal ports of 1B7T antenna array is ≥ 36 dB and of 1B19T antenna array is ≥ 32 dB over entire bandwidth. Simulated gain vs. frequency plot for port1 of 1B7T and 1B19T dual polarized space-fed arrays are shown in Figure 4(b). The 1B7T array has maximum gain of 15.3 dBi at 5.8 GHz and 1B19T array has maximum gain of 18.1 dBi at 5.85 GHz.

Simulated E and H plane radiation patterns at 5.6 GHz, 5.8 GHz and 6.0 GHz for port1 of 1B7T antenna array with infinite ground plane are shown in Figure 5. The 1B7T antenna array has half power beam width (HPBW) of approximately 30 degrees in both E and H planes. The cross-polar levels are ≤ -33 dB and side lobe levels (SLL) are ≤ -16 dB in both the planes for entire frequency band. Simulated E and H plane radiation patterns at 5.7 GHz, 5.8 GHz and 6.1 GHz for port1 of 1B19T antenna array with infinite ground plane are shown in Figure 6. The 1B19T antenna array has HPBW of approximately 18 degrees, cross-polar levels ≤ -30 dB and SLL ≤ -9 dB in both E and H planes for entire frequency band. The E plane radiation pattern of antenna array has small asymmetry due to radiation from bottom microstrip feed lines located at one edge of the radiating element. Variation in SLL is observed due to small difference in reflection coefficient phase across frequency band. The

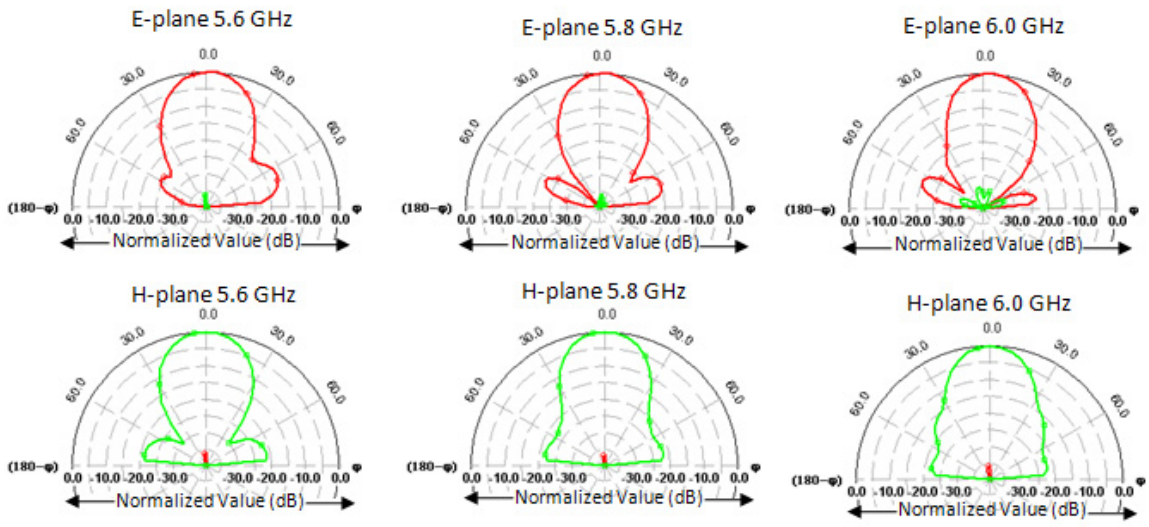

Figure 5. Simulated E and H plane radiation patterns for port1 of 1B7T dual polarized space-fed antenna array at 5.6 GHz, 5.8 GHz and 6.0 GHz.

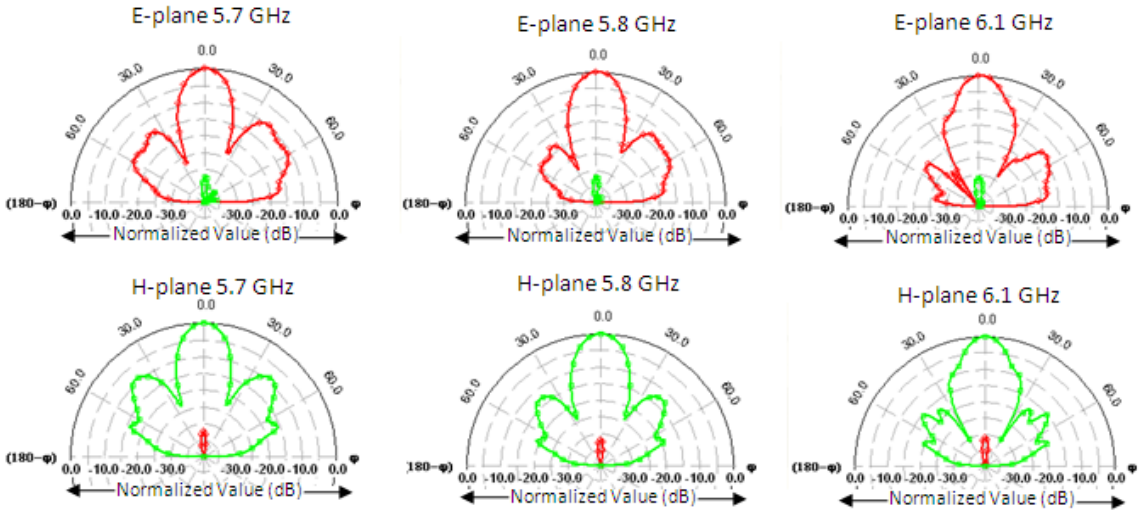

Figure 6. Simulated E and H plane radiation patterns for port1 of 1B19T dual polarized space-fed antenna array at 5.7 GHz, 5.8 GHz and 6.1 GHz.

performance characteristics for port2 of antenna arrays are same as that of port1 due to symmetry of antenna configurations. The comparison of performances of 1B7T and 1B19T dual polarized antenna configurations is given in Table 2.

The 1B19T dual polarized space-fed antenna array is fabricated with a finite ground plane of 200 mm × 200 mm as shown in Figure 7. To reduce back lobe radiation due to fringing field of top layer parasitic elements, the space-fed antenna arrays are backed by large ground planes. The dual microstrip feed lines with quarter wave transformer are fabricated on bottom substrate. The bottom radiating element is placed in suspended configuration with air gap of 2.5 mm. The array of parasitic elements is fabricated on top substrate and placed in inverted configuration using support of Teflon rods at a height of $3\lambda_0/2$ from bottom radiating element.

The measured S-parameters vs. frequency plots for port1 of 1B19T dual polarized space-fed antenna array are shown in Figure 8(a). The antenna has measured RL $\leq$ 10 dB bandwidth of 620 MHz (5.68 GHz

Table 2. Comparison of performance of 1B7T and 1B19T space-fed antenna arrays.

Performance Parameters	1B7T Array	1B19T Array
VSWR ≤ 2 bandwidth (MHz)	400	640
Maximum isolation (dB)	44	47
Isolation for entire bandwidth (dB)	≥ 36	≥ 32
Max. Gain (dBi)	15.3	18.1
Cross-polar level at 5.8 GHz (dB)	≤ -36	≤ -31
Side lobe level at 5.8 GHz (dB)	≤ -20	≤ -14
E-plane HPBW at 5.8 GHz (degrees)	-13.4 to 15.6	-8.2 to 9.9
H-plane HPBW at 5.8 GHz (degrees)	-15.5 to 15.5	-9.1 to 9.1

to 6.3 GHz). The measured frequency band has small shift towards higher frequency due to fabrication errors. Measured isolation between two orthogonal ports is ≥ 32 dB with peak isolation of 59 dB at 5.6825 GHz. Measured gain vs. frequency plot for port1 of 1B19T dual polarized space-fed antenna array is shown in Figure 8(b). The antenna array has maximum measured gain of 17.8 dBi at 5.9 GHz, which is 0.3 dB less than the simulated gain due to finite ground plane. The measured E and H planes radiation patterns of 1B19T antenna array at 5.8 GHz are shown in Figure 9. The antenna array has measured HPBW of 17 degrees in E-plane and 16 degrees in H-plane. The antenna array has measured SLL ≤ -13 dB and cross-polar levels ≤ -29 dB in E and H planes. The measured S-parameters, gain and radiation properties for port2 of antenna array are similar to that of port1 due to symmetry of

(a) (b)

Figure 7. Fabricated 1B19T dual polarized space-fed antenna array, (a) bottom ground plane with dual feeds and (b) integrated antenna array with top parasitic elements.

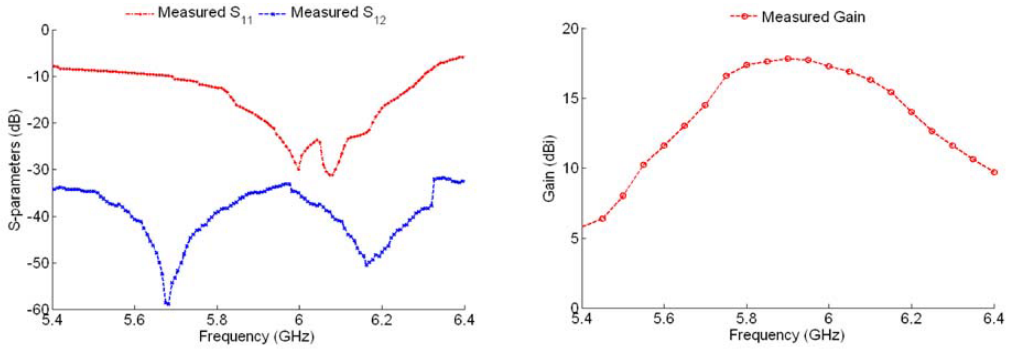

(a) (b)

Figure 8. Measured (a) S-parameters vs. frequency and (b) gain vs. frequency plots for port1 of 1B19T dual polarized space-fed antenna array.

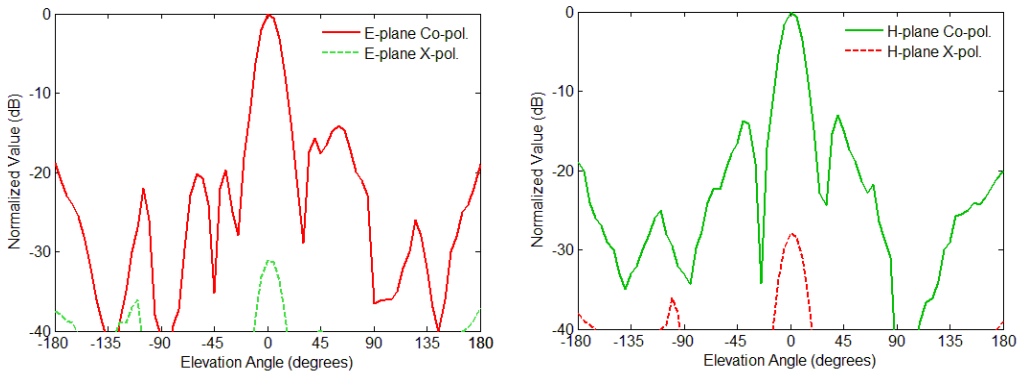

Figure 9. Measured (a) E-plane and (b) H-plane radiation patterns at 5.8 GHz for port1 of 1B19T dual polarized space-fed antenna array.

Table 3. Comparison of proposed 1B19T space-fed antenna array with other reported results.

Ref.	No. of elements	Freq. (GHz)	% BW	Isolation (dB)	X-pol. (dB)
[14]	16	12	$P_1 = 1.7$, $P_2 = 4$	≥ 30	≤ -22
[15]	4	5.8	14	≥ 30	≤ -20
[16]	2	0.89	19.8 (RL -14 dB)	≥ 36	≤ -15
[17]	16	5.505	2.3	≥ 40	-
[18]	36	5.8	$P_1 = 26$, $P_2 = 28$	≥ 30	-
[19]	8	1.5	20	≥ 30	≤ -25
[20]	4	2.35	18	≥ 30	≤ -22
[21]	16	5.5	19.5	≥ 20	≤ -19.2
Proposed Array	19	5.8	10.7	≥ 32	≤ -29

antenna configuration for two ports.

The 1B19T dual polarized space-fed antenna array performance is compared with other proposed configurations of dual polarized antenna arrays in Table 3. The proposed space-fed antenna array has advantage of simple array design achieving broad bandwidth for two orthogonal ports. The antenna array has high isolation between two orthogonal ports and smaller cross-polar levels as compared to antenna arrays proposed in literature. The smaller cross-polar levels of proposed dual polarized antenna array is due to absence of feed networks for arrays. This results in no spurious radiation from feed achieving improvement in both isolation between two orthogonal ports and smaller cross-polar levels in E and H-planes.

4. CONCLUSION

This paper presents novel design of broadband dual polarized antenna arrays using electromagnetically coupled bottom radiating element and space-fed arrays of parasitic elements. The antenna arrays are designed without feed network for the excitation of two orthogonal modes of the array of parasitic elements resulting in improvement in isolation between two orthogonal ports. The absence of feed network also reduces spurious radiation from orthogonal feeds achieving smaller cross-polar levels. The space-fed dual polarized antenna array with one bottom radiating element and 19 top parasitic elements (1B19T) is fabricated and its performance is measured. The 1B19T antenna array has measured bandwidth of 10.7% and isolation ≥ 32 dB over entire bandwidth with maximum isolation of 59 dB. For finite ground plane of 200 mm $\times$ 200 mm, measured maximum gain of the antenna array is 17.8 dBi and cross-polar levels ≤ -29 dB.

REFERENCES

1. Vaughan, R. G. and J. B. Anderson, "Antenna diversity in mobile communications," *IEEE Trans. Vehicular Techn.*, Vol. 36, 149–172, 1987.
2. Oestges, C., B. Clerckx, M. Guillaud, and M. Debbah, "Dual-polarized wireless communications: From propagation models to system performance evaluation," *IEEE Trans. Wireless Comm.*, Vol. 7, No. 10, 4019–4031, 2008.
3. Erceg, V., H. Sampath, and S. C. Erceg, "Dual-polarization vs. single-polarization MIMO channel measurement results and modeling," *IEEE Trans. Wireless Comm.*, Vol. 5, No. 1, 28–33, 2006.
4. Giulli, D., "Polarization diversity in radars," *Proc. of the IEEE*, Vol. 74, No. 2, 245–269, 1986.
5. Wang, Y. and V. Chandrasekar, "Polarization isolation requirements for linear dual-polarization weather radar in simultaneous transmission mode of operation," *IEEE Trans. Geoscience and Remote Sensing*, Vol. 44, No. 8, 2019–2028, 2006.
6. Wong, H., K.-L. Lau, and K.-M. Luk, "Design of dual-polarized L-probe patch antenna arrays with high isolation," *IEEE Trans. Antennas Propag.*, Vol. 52, No. 1, 45–52, 2004.
7. Lai, H.-W. and K.-M. Luk, "Dual polarized patch antenna fed by meandering probes," *IEEE Trans. Antennas Propag.*, Vol. 55, No. 9, 2625–2677, 2007.
8. Wong, K. L., H.-C. Tung, and T.-W. Chiou, "Dual-polarized planar antenna fed by dog-bone slots," *International Conference on Antennas and Propagation*, 45–48, Apr. 2001.
9. Gao, S. and A. Sambell, "Dual polarized broad-band microstrip antennas fed by proximity coupling," *IEEE Trans. Antennas Propag.*, Vol. 53, No. 1, 526–530, 2005.
10. Wong, K. L., H.-C. Tung, and T.-W. Chiou, "Broadband dual-polarized aperture-coupled patch antennas with modified H-shaped coupling slots," *IEEE Trans. Antennas Propag.*, Vol. 50, No. 2, 188–191, 2002.
11. Wong, K. L. and T.-W. Chiou, "Broad-band dual-polarized patch antennas fed by capacitively coupled feed and slot-coupled feed," *IEEE Trans. Antennas Propag.*, Vol. 50, No. 3, 346–351, 2002.
12. Lau, K. L. and K. M. Luk, "A novel wideband circularly polarized patch antenna based on L-probe and aperture coupling techniques," *IEEE Trans. Antennas Propag.*, Vol. 53, No. 1, 577–580, 2005.
13. Ononchimeg, S., J.-H. Bang, and B.-C. Ahn, "A new dual-polarized gap-fed patch antenna," *Progress In Electromagnetics Research C*, Vol. 14, 79–87, 2010.
14. Zhong, S.-S., X.-X. Yang, S.-C. Gao, and J.-H. Cui, "Corner-fed microstrip antenna element and arrays for dual-polarization operation," *IEEE Trans. Antennas Propag.*, Vol. 50, No. 10, 1473–1480, 2002.
15. Gao, S. and A. Sambell, "Low-cost dual polarized printed array with broad bandwidth," *IEEE Trans. Antennas Propag.*, Vol. 52, No. 12, 3394–3397, 2004.
16. Lau, K. L. and K.-M. Luk, "A wideband dual-polarized L-probe stacked patch antenna array," *IEEE Antennas Wireless Propagat. Lett.*, Vol. 6, 529–532, 2007.
17. Acimovic, I., D. A. McNamara, and A. Petosa, "Dual-polarized microstrip patch planar array antennas with improved port-to-port isolation," *IEEE Trans. Antennas Propag.*, Vol. 56, No. 11, 3433–3439, 2008.
18. Mishra, P. K., D. R. Jahagirdar, and G. Kumar, "An array of broadband dual polarized electromagnetically coupled microstrip antennas," *Progress In Electromagnetics Research C*, Vol. 44, 211–223, 2013.
19. Chakrabarti, S., "Development of shared aperture dual polarized microstrip antenna at L-band," *IEEE Trans. Antennas Propag.*, Vol. 59, No. 1, 294–297, 2011.
20. Jiang, X., Z. Zhang, Y. Li, and Z. Feng, "A planar wideband dual-polarized array for active antenna system," *IEEE Antennas Wireless Propagat. Lett.*, Vol. 13, 544–547, 2014.
21. Zhao, X.-Li, J. Jin, J.-C. Cheng, and L.-G. Liang, "A wideband dual-polarized array antenna with conical elements for Wi-Fi/WiMAX application," *IEEE Antennas Wireless Propagat. Lett.*, Vol. 13, 1609–1612, 2014.
22. IE3D EM Design System, Version 15.0, Mentor Graphics Corp., Wilsonville, USA, 2010.